



PHOTOCATALYTIC EFFICIENCY OF TiO₂ IN BIOTEMPLATES FORM IN THE DECOLORATION OF ORGANIC DYE AND INHIBITION OF *E. COLI* GROWTH

Siara Silvestri^{a*}, Beatriz Batista^b, Juliana Schultz^c, Adelaide Almeida^b, Antonio S. Mangrich^{c,d}, Bruno Szpoganicz^a

^aDepartment of Chemistry,
Federal University of Santa Catarina, 88040-900 Florianópolis, SC, Brazil
siarasilvestri@gmail.com; bruno.s@ufsc.br

^bDepartment of Biology and CESAM,
Aveiro University, 3810-193 Aveiro, Portugal
beatrizbatista@ua.pt; aalmeida@ua.pt

^cDepartment of Chemistry, Federal University of Paraná, 81531-980 Curitiba, PR, Brazil
julianaschultz@yahoo.com.br

^dNational Institute of Science and Technology - Energy and Environment (INCT E&A) Salvador, BA, Brazil
asmangrich@gmail.com

ABSTRACT

Anatase TiO₂ is widely used for pollutant degradation due to its photocatalytic property. Exposure of the surface to UV radiation (sunlight or artificial) generates an electron-hole pair that is responsible for the formation of free radicals such as O₂^{•-} in the presence of atmospheric oxygen and HO[•] in the presence of water. Biomorphic TiO₂ plates were produced by infiltration of paper with titanium isopropoxide (TTiP) solution followed by hydrolysis in NH₄OH and calcination at temperatures up to 600-1000 °C, as a new way of fixing TiO₂ with the aim of delaying the phase transition from anatase (photoactive) to rutile (inactive). In order to study the effect of addition of zirconia as a dopant on the microstructure and the phase transition from anatase to rutile, the same procedure was used, but with the addition of 5% (m/m) of ZrO(NO₃)₂ to TTiP. The biomorphic materials were characterized by XRD, specific surface area measurement (using the BET method), EPR, and SEM. Their photocatalytic efficiencies were evaluated in the decoloration of Orange II dye and the inhibition of growth of *E. coli* bioluminescent bacteria. Using 5% Zr-doped TTiP, with calcination at 800 °C, bacterial growth was reduced by 23% after 180 minutes, and 70% dye decoloration was achieved in 30 hours.

Keywords

Titanium biotemplate, organic dye, microbial inactivation.

Council for Innovative Research

Peer Review Research Publishing System

Journal: Journal of Advances in Chemistry

Vol. 12, No. 3

editor@cirjac.com

www.cirjac.com

INTRODUCTION

When the TiO₂ anatase structure is exposed to UV radiation, electrons are driven to an electronically excited state. As a result, there is the formation of reactive free radicals, especially hydroxyl and superoxide, and one electron-hole pair (e⁻/h⁺) in the valence shell. These features result in an oxidizing material that is capable of degrading organic molecules adsorbed on its surface. The photocatalytic activity of TiO₂ mainly depends on the contents of the anatase and rutile crystalline phases, as well as the specific surface area.^{1,2} The anatase phase is irreversibly transformed to rutile at temperatures in the region of 600 °C.¹

Most studies of photocatalytic TiO₂ employ TiO₂ in powder form (one-dimensional). Alternatively, the biotemplate method involves the generation of a three-dimensional ceramic material that mimics the morphological structure of an organic matrix, and enables liquid ceramic precursors to be used for infiltrating the organic matrix. Hydrolysis of the precursors, followed by a calcination step for the removal of organics, results in the formation of a ceramic plate with the morphological characteristics of the organic matrix.³⁻⁷

The photocatalytic efficiency of TiO₂ can be evaluated by the decoloration of organic dyes, the degradation of atmospheric pollutants, and the inactivation of microorganisms. The azo dyes (Orange II, Methyl Red, and Methyl Yellow) are highly toxic carcinogenic compounds that are used in textile industry dyeing processes. Discharges of the wastewater can cause serious environmental and health problems.^{8,9} For this reason, destruction of the dyes present in wastewater is a high priority.¹⁰ The absorption of light by Orange II occurs between 480 and 490 nm, corresponding to a blue-green color, and the complementary color (the observed color) is orange. This absorption is due to the extensive conjugated single and double bonds, with the aromatic rings of the molecule linked with an azo bond (N=N) (**Fig. 1**). The azo bonds are the most active links in azo dye molecules and can be oxidized by hydroxyl radicals, or be reduced by electrons in the conduction band. The cleavage of N=N bonds leads to dye decoloration.^{8,9}

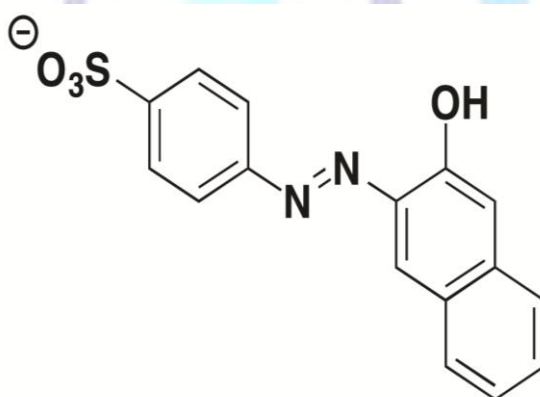


Figure 1: Structural representation of Orange II dye.

Photoinduced inactivation of microorganisms by anatase TiO₂ is known to involve the inhibition of microbial cell multiplication.^{11,12} One of the latest reviews concerning the antimicrobial activity of TiO₂ is provided by Foster et al.,¹² where the mechanism of cell death is described as involving degradation of the cell wall and the cytoplasmic membrane due to the formation of reactive oxygen species such as hydroxyl radicals and hydrogen peroxide.

Although *E. coli* is a commensal bacterium, several strains can cause diseases such as gastrointestinal and urinary tract infections, even in the most robust human hosts.¹¹ The use of antibacterial self-sterilizing TiO₂ plates could be a valuable strategy against these kinds of bacterial strains.

In this work, paper was used as an organic biotemplate matrix to produce biomorphic TiO₂ plates with morphology similar to that of the biotemplate, as a green and innovative alternative for fixation of TiO₂. The great advantage of obtaining pure, thin, and flat plates of TiO₂ is that these substrates do not suffer from the disadvantages of TiO₂ powder, which becomes dispersed and is hard to recover after its use in photocatalysis.¹³ Another advantage is the high surface/volume ratio, because the photocatalysis occurs on the surface of the material. The photocatalytic efficacies of these new materials were tested using an innovative real-time bioluminescent method for analysis of bacterial activity, as well as by organic azo dye decoloration.



2. EXPERIMENTAL

2.1. Production of plates

Addition of 5 wt% $ZrO(NO_3)_2$ to titanium isopropoxide solution (TTiP, Aldrich, 97%) was followed by homogenization under magnetic stirring. Rectangles of paper (850 g m^{-2} , Canson Arches TF, France) were used as biotemplates for the production of TiO_2 plates. The biotemplates were placed in TTiP or Zr-doped TTiP solutions for infiltration, then removed from the solutions after 1 h and transferred to 30% NH_4OH (Synth) for hydrolysis for 1 h under magnetic stirring. The biotemplates were removed from the NH_4OH and air-dried at room temperature for 24 h. Subsequently, they were calcined for 30 min in a muffle furnace at temperatures between 600 and 1000 °C, using a heating rate of 10 °C min^{-1} .

2.2. EPR analyses

The spin trapping method was used in electron paramagnetic resonance (EPR) measurements of HO^\bullet radicals. A 0.2 M solution of DMPO (5,5-dimethyl-1-pyrroline N-oxide, Aldrich) was prepared with high purity water (Mill-Q system, Millipore) and was used to homogenize the plates, forming a slurry. This slurry was introduced into a glass capillary tube, which was then placed in a quartz EPR tube. The WIN EPR program (Bruker) was used for the acquisition and manipulation of the EPR spectra.

2.3. Experimental setup

Evaluation of the photocatalytic efficiency of TiO_2 in the degradation of organic dye employed a black light lamp (F15, GE), with 10 mW m^{-2} UV irradiation of the vessel containing the sample. One vessel was filled with 100 mL of dye solution (14 mg L^{-1}), and another contained 100 mL of the dye solution and the TiO_2 (9 cm^2) biotemplate. The latter vessel was covered with aluminum foil to protect it from UV radiation. All the experiments were conducted under the same conditions: $10\pm 0.5\text{ mW m}^{-2}$ irradiation, measured with a lux meter (MRU-201, Instrutherm) at 10 cm from the vessel; pH 7; temperature of $23\pm 5\text{ °C}$. Aliquots were withdrawn every hour for measurement of absorbance using a Lambda 750 spectrophotometer (PerkinElmer). The duration of the test was 30 h, and the decoloration efficiency (ξ) of Orange II dye was calculated using Eq. 1:

$$\xi (\%) = \frac{A_0 - A_f}{A_0} \times 100 \quad (1)$$

where A_0 is the initial absorbance and A_f is the absorbance after exposure to UV irradiation at $\lambda = 486\text{ nm}$.¹⁴ The products resulting from Orange II dye decoloration were evaluated by removing aliquots of the solutions at the beginning, middle, and end of the test, for analysis using liquid chromatography-mass spectrometry (Model 1100 LC/MS, Agilent).

Alves et al.¹⁵ described a fast and simple method for monitoring the photoinactivation of *Escherichia coli*, involving the use of recombinant bioluminescent bacteria. *Escherichia coli* cells were transformed with luxCDABE genes from the marine bioluminescent bacterium *Vibrio fischeri*, and the recombinant bioluminescent indicator strain was used to assess, in real time, the effect of anatase TiO_2 plates under artificial irradiation.

In the present work, bacterial cultures were cultivated overnight, following the procedure of Alves et al.,¹⁵ followed by ten-fold dilution in phosphate buffered saline (PBS) to a final concentration of 10^6 CFU mL^{-1} . This bacterial suspension was equally distributed into sterilized 100 mL glass beakers. Two plates ($2 \times 3\text{ cm}$, 60 mg) of the TiO_2 under study were then added, giving a total volume of 10 mL. The samples were protected from light with aluminum foil and incubated for 10 min at 25 °C, with stirring at 100 rpm. Light and dark controls were included in the experiments. In the case of the light control, no plates were added, but the beaker was exposed to the same irradiation protocol. For the dark control, the plates were added to the beaker, which was then shielded with aluminum foil.

The samples were exposed to UV irradiation (290–400 nm) at intensity of 20 W m^{-2} . Lamps were turned on 30 min prior to each experiment, in order to stabilize the irradiance. Every 15 min, a 1 mL aliquot was removed from each beaker and the bioluminescence was measured using a luminometer (GloMax 20/20) to determine the degree of photocatalytic inactivation. Three replicates were used in each experiment, which was repeated three times. In each experiment, control samples (using cells in the absence of TiO_2) were irradiated under the same conditions.

3. RESULTS AND DISCUSSION

X-ray diffraction analysis was used to identify the crystalline phases present in the materials calcined between 600 and 1000 °C, as well as to estimate their relative proportions (Fig. 2).

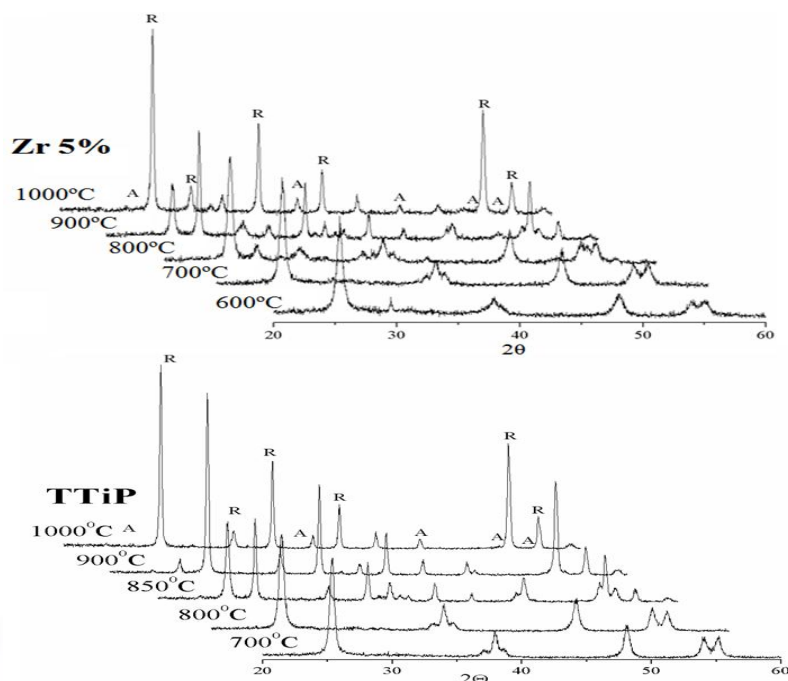


Figure 2: X-ray diffractograms for plates prepared from TTiP and 5% Zr-doped TTiP, calcined between 600 and 1000 °C. A = anatase; R = rutile.

With heating, the intensities of the characteristic peaks of anatase increased significantly, accompanied by reduced widths. Below 800 °C, only the anatase phase was present. The rutile phase appeared at 850 °C, and the anatase and rutile phases then co-existed at temperatures up to 900 °C. At 1000 °C, only the rutile phase was present. Addition of the dopant did not result in the formation of any additional crystal phases.

Table 1 presents the evolution of crystallite size with calcination temperature, as calculated using the Scherrer equation. The anatase crystallites became larger as the temperature increased, and the formation of rutile was observed when the particles reached ~20 nm.

Table 1: Crystallite size, anatase and rutile contents, surface area, and band gap of biotemplates calcined at different temperatures.

Sample	Content (%)		Surface area ($m^2 g^{-1}$)	Crystallite size (nm)		Band gap (eV)
	Anatase	Rutile		Anatase	Rutile	
TTiP 700 °C	100	0	11.02	19.4	-	3.12
TTiP 800 °C	92.4	7.6	8.91	19.6	38.9	2.95
TTiP 850 °C	48.1	51.9	6.40	29.1	38.9	2.97
TTiP 900 °C	6.7	93.3	4.19	38.8	43	3.02
TTiP 1000 °C	0	100	2.83	-	45.4	3.00
Zr 5% 800 °C	81.6	18.4	16.116	19.57	25.55	2.95
Zr 5% 900 °C	7.6	92.4	7.193	22.62	40.89	-
Zr 5% 1000 °C	0	100	4.356	-	44.44	-

The lattice parameters were altered with increase of calcination temperature and doping. The specific surface area decreased with increasing calcination temperature, with the highest specific surface area shown by the 5% Zr-doped sample calcined at 800 °C. Considering the results of the XRD analyses and the lattice parameters, it was decided to use the doped and undoped plates calcined at 800 °C, which showed the lowest band gap values and therefore required less energy for the generation of free radicals.

The morphologies of the samples are shown in **Fig. 3**. In all cases, typical organic shapes were present, as expected. **Fig. 3a** shows the microstructure of the organic matrix. **Figs. 3b** and **3c** show the samples prepared with undoped TTiP and calcined at 800 °C and 1000 °C, respectively. **Fig. 3d** shows the 5% Zr-doped TTiP sample calcined at 800 °C. At high calcination temperatures, the cellulose fibers were combusted, with TiO₂ remaining and forming similar shapes. There were no substantial sintering reactions, at least up to 450 °C, but the particles tended to be coarse and adhered.

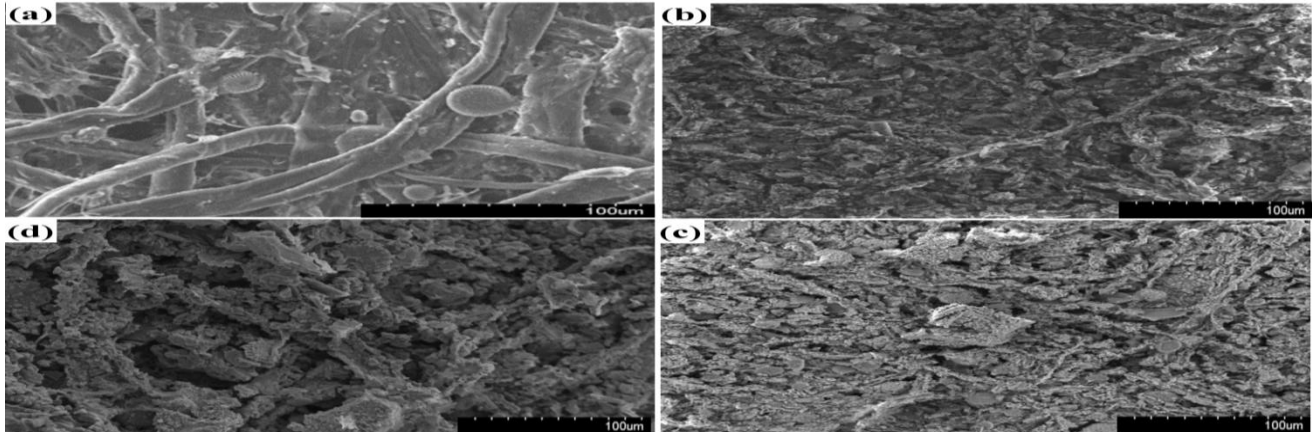


Figure 3: Scanning electron micrographs of the biotemplate before infiltration (a), and samples prepared with (b) undoped TTiP and calcined at 800 °C, (c) undoped TTiP and calcined at 1000 °C, and (d) 5% Zr-doped TTiP and calcined at 800 °C.

The ability of the anatase and rutile plates to produce hydroxyl radicals upon photoexcitation with UV radiation in aqueous suspensions was monitored by EPR, using DMPO as a spin-trapping agent, producing a stable free radical product (spin adduct). DMPO was selected because of its low redox activity and its ability to produce EPR spectra that reflect the radical species present.^{16,17} After continued exposure of the TiO₂ suspensions, a quartet of lines with peak height proportions of 1:2:2:1 was obtained, typical of the ⁵DMPO-OH signal (**Fig. 4**). The DMPO molecule was sufficiently photostable under the experimental conditions employed.^{18,19} No radical formation was detected in the absence of illumination.

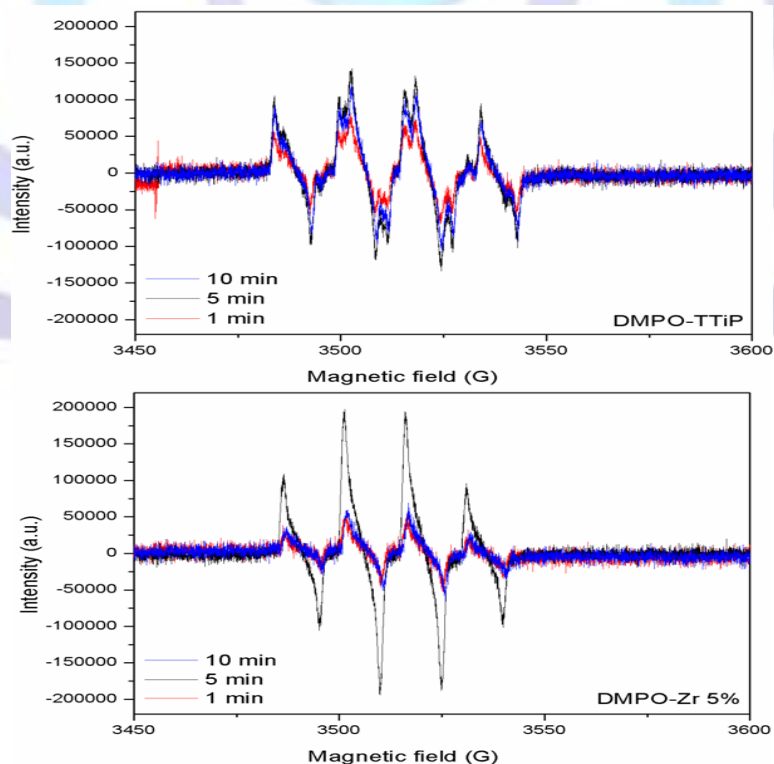


Figure 4: EPR spectra of TTiP and 5% Zr-doped TTiP plates calcined at 800 °C, using DMPO and irradiation with UV light for 1, 5, and 10 min.

The quantity of HO[•] radicals generated by the plates increased with irradiation time, and the plate doped with Zr produced more HO[•] radicals than the plate produced without doping. The high generation of radicals by the plates was probably related to their high specific surface areas. The decoloration percentages achieved by the plates produced using TTiP and calcined at different temperatures are compared in **Fig. 5**.

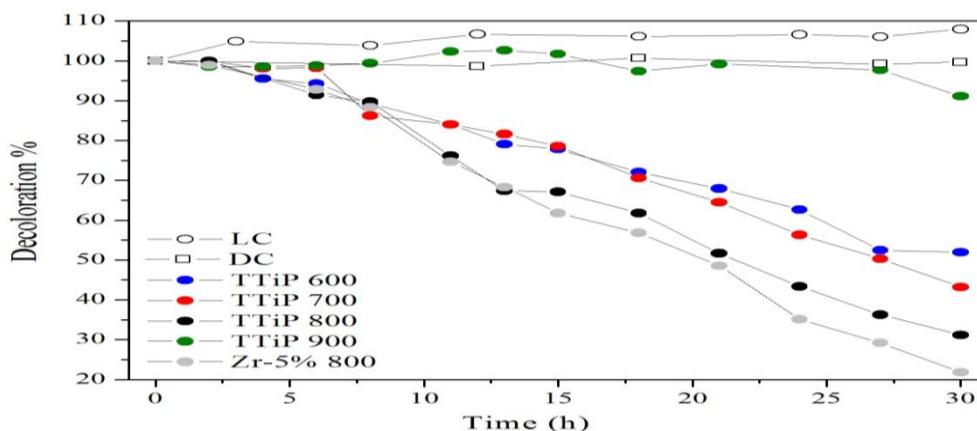


Figure 5: Decoloration of Orange II dye by TiO₂ plates produced using TTiP and calcined at temperatures between 600 and 900 °C. LC: light control; DC: dark control.

The decoloration values obtained for the light control showed that UV radiation alone did not cause any dye decoloration, and an increase in the absorbance values could be explained by the evaporation of water from the solution during the test. The values obtained for the dark control indicated that TiO₂ was unable to decolor the dye in the absence of UV radiation. The plate doped with Zr showed the best decoloration percentage, which reached 80% after 30 h. Among the undoped plates, the best decoloration percentage was achieved with the sample calcined at 800 °C (70% after 30 h).

Orange II dye exhibits phototropism and mainly exists in two tautomeric forms (the azo and hydrazone forms) (**Fig. 6**). However, the hydrazone form is predominant in aqueous solution. Photocatalytic degradation leads to decoloration of the solution by decreasing the absorption band, following adsorption of the dye on the surface of the photocatalyst via the oxygen of the hydrazone and the two oxygen atoms of the sulfonate group.

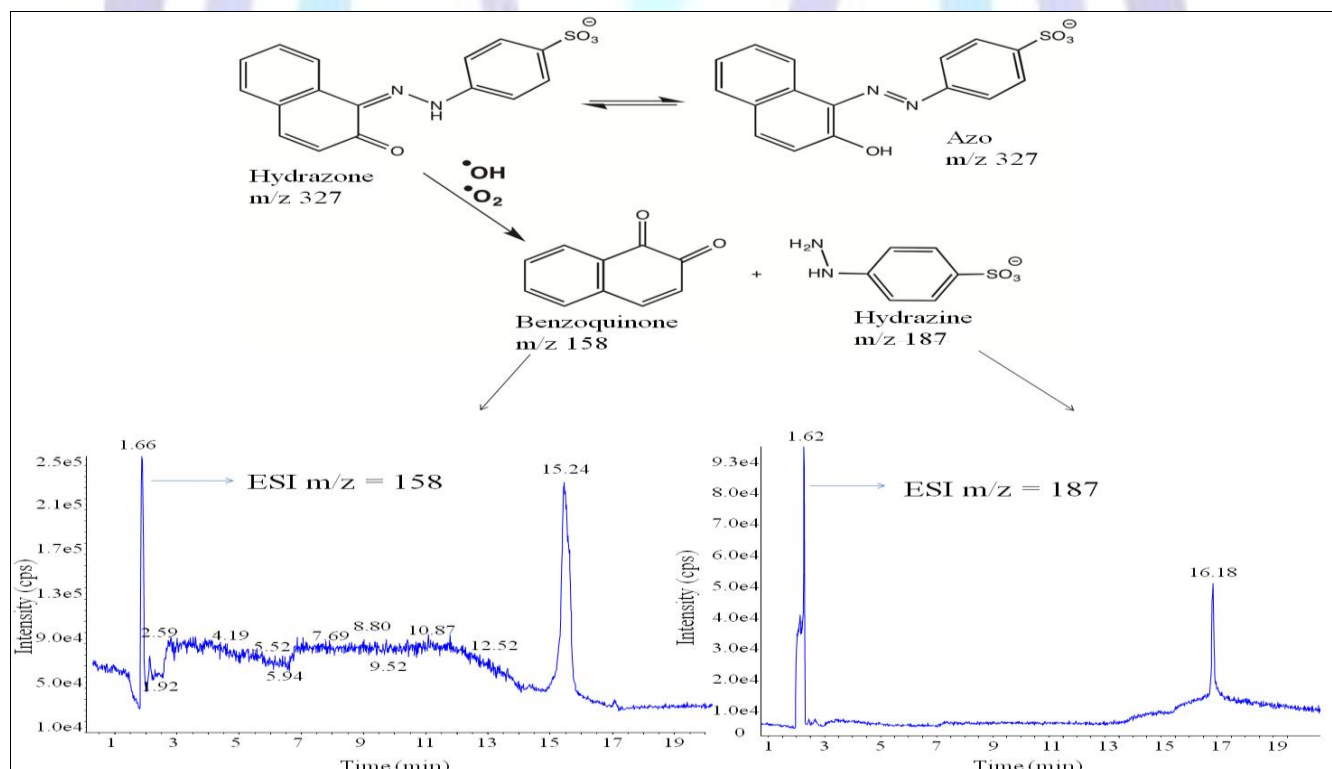


Figure 6: Mechanism of decoloration of Orange II dye.

Interaction with the radicals generated in the photocatalytic process cleaved the azo bond of the dye molecule (**Fig. 6**), as shown by the analysis using liquid chromatography coupled with mass spectrometry. This step resulted in decoloration of the solution, but was not accompanied by any significant reduction in chemical oxygen demand.²⁰

For evaluation of the intermediate species generated in the degradation process, aliquots of sample were analyzed at the start of the test and after 15 and 30 h of irradiation. As shown in **Fig. 7**, the concentration of Orange II decreased as the hydrazine and benzoquinone fragments were formed (**Fig. 6**).

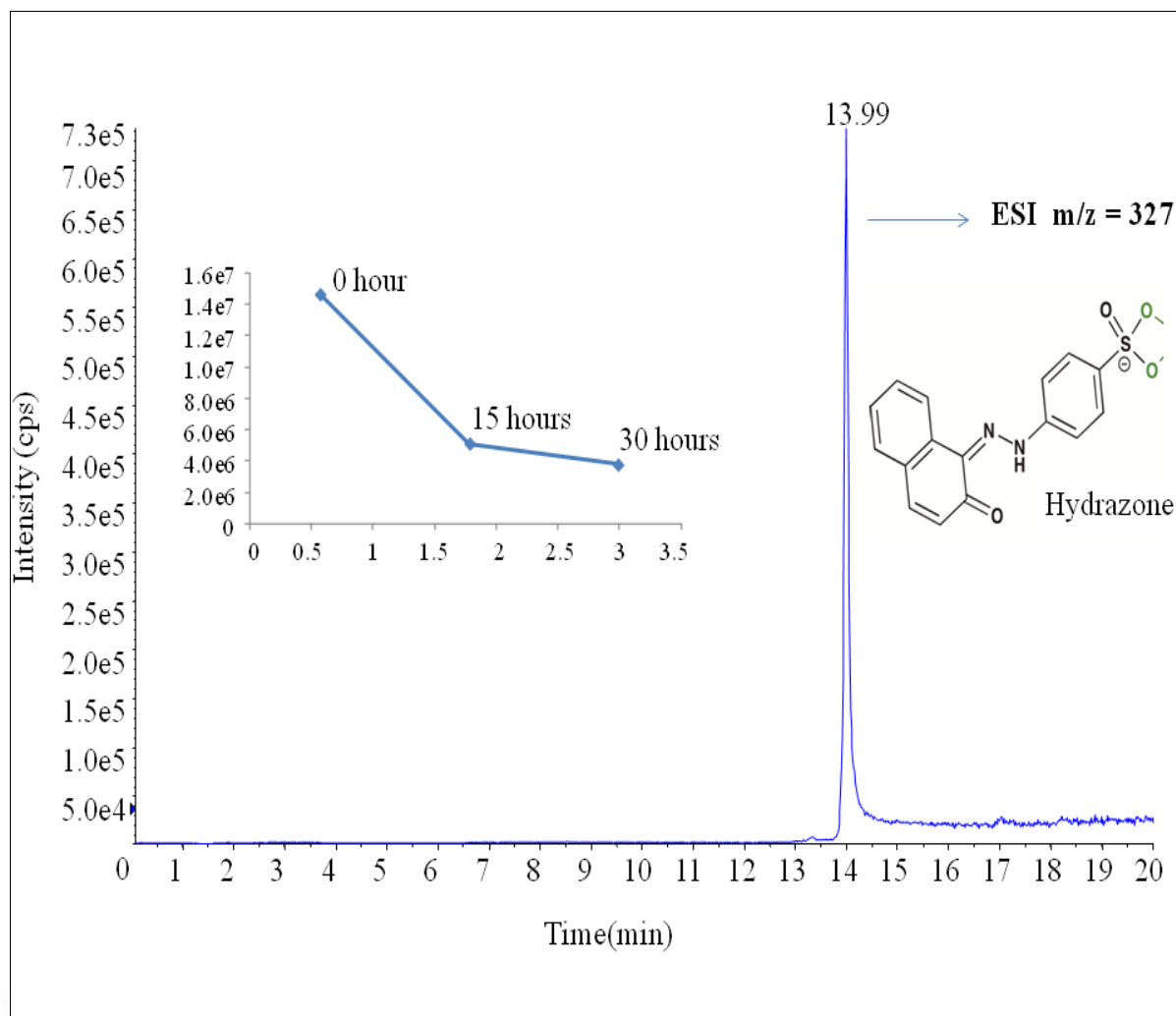


Figure 7: Liquid chromatography spectrum showing the decreased concentration of Orange II dye after 30 h of the test.

All the aqueous wastes generated in the experiments were decolorated using the plates developed in this work under UV light irradiation, until all the solutions were colorless, hence avoiding any discharges of toxic materials.

The antibacterial tests were performed using a control with no titania present, and using 6 mg of the TiO_2 plates per mL, with and without UV irradiation. The results showed that the undoped TiO_2 presented low activity under UV irradiation (**Fig. 8a**), which was comparable to the decrease in the bacterial concentration induced by UV light alone. Under UV irradiation, the bacterial concentration was reduced by 9% after 90 min, while a reduction of around 11% was obtained in the presence of the TiO_2 plates, under the same irradiation conditions. When the tests were performed in the dark, however, the bacterial concentration remained constant. This indicated that the growth of *E. coli* was affected by UV radiation. However, use of the 5% Zr-doped TiO_2 plate resulted in greater bacterial inactivation. The results of the experiments performed under UV irradiation and in the dark are shown in **Fig. 8b**.

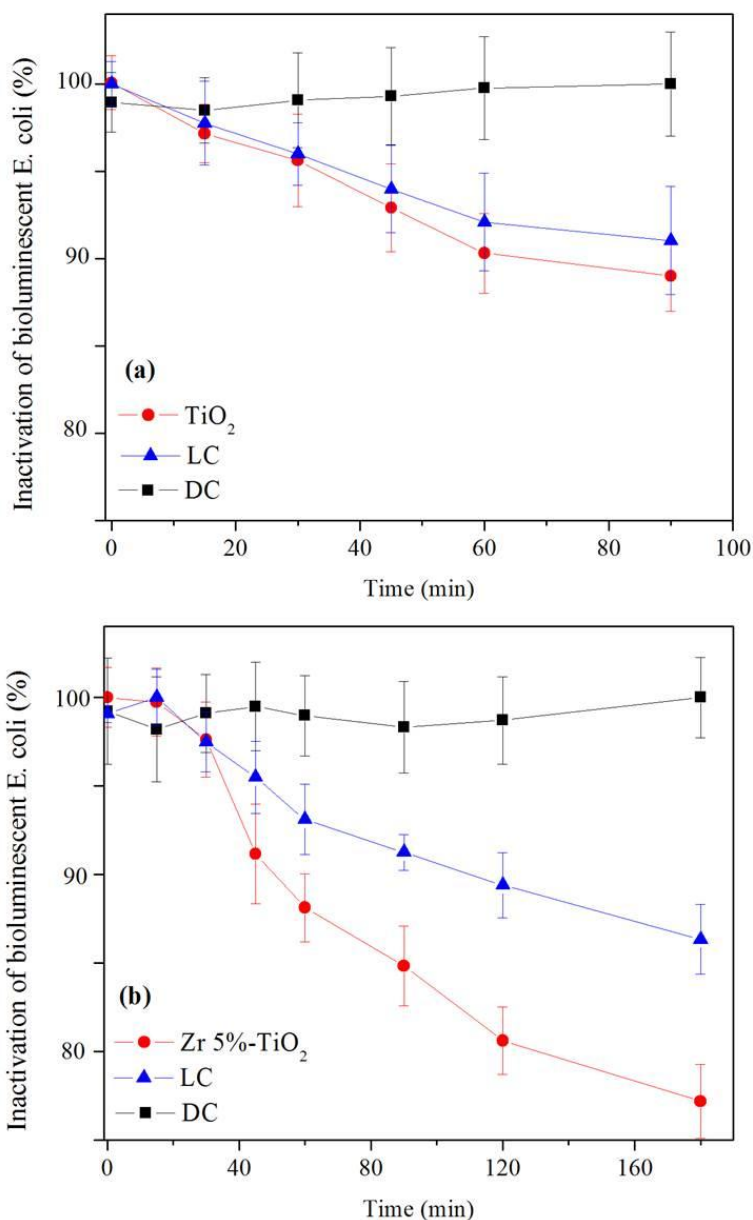


Figure 8: Antibacterial tests with (a) undoped TTiP plate and (b) 5% Zr-doped TiO₂ plate, calcined at 800 °C.

The addition of Zr as a dopant increased the antibacterial properties of the material, in agreement with the observed photocatalytic activity, with 23% inactivation after 180 min. This could be explained by the influence of Zr in reducing the size of the rutile crystallites, hence increasing the specific surface area, leading to higher photocatalytic activity. Tests performed under different experimental conditions can make comparisons difficult, and differences in the antibacterial action of TiO₂-based materials can be due to the effects of various parameters, such as morphology/area and (in the case of nanoparticles) average dimensions as well as shape.¹² The mechanisms causing bacterial inactivation under light irradiation are not completely understood, although they are likely to involve damage to the cell membrane and alterations in cell morphology caused by the light-generated radical species.²¹ In this mechanism, the complexity and the density of the cell wall of the microorganisms play a key role in their resistance to the antibacterial material.

4. CONCLUSIONS

The plates produced in this work offer excellent potential for use in practical applications, benefitting from their three-dimensional hierarchical structures with high surface-to-volume ratios, which ensure efficient diffusion pathways for the capture and degradation of pollutant species. Furthermore, an interconnected structure not only provides superior photocatalytic performance, but also from a practical point of view enables easier removal of the photocatalyst from the environment. The use of zirconium as a dopant in biomorphic TiO₂ plates was effective in reducing the size of the crystallites and increasing the surface area of the plates, hence improving the photocatalytic activity. The TiO₂ plates



provided effective photoinactivation of *E. coli*. This approach could be used as a screening method for *in vitro* bacterial photoinactivation studies, as well as for evaluating the effectiveness of novel materials. We intend to continue this study using plates with other dopants such as Ba²⁺ and La³⁺, and the production of plates starting from titanium tetrachloride.

ACKNOWLEDGMENTS

The authors gratefully acknowledge the financial support provided by CNPq and CAPES, INCT catálise and LACFI.

REFERENCES

1. Hanaor, D. A. H., Sorrell, C. C., (2011). Review of the anatase to rutile phase transformation. *Journal of Materials Science*, 46 855–874.
2. Henderson, M. A., (2011). A surface science perspective on TiO₂ photocatalysis. *Surface Science Reports*, 66 (6) 185–297.
3. Huang, J., Kunitake, T., (2003). Nano-precision replication of natural cellulosic substances by metal oxides. *Journal of the American Chemical Society*, 125 (39) 11834–11835.
4. Ota, T. et al., (2000). Porous titania ceramic prepared by mimicking silicified wood. *Journal of the American Chemical Society*, 83 (6) 1521–1523.
5. Popovska, N., Streitwieser, D. A., Xu, C., Gerhard, H., (2005). Paper derived biomorphic porous titanium carbide and titanium oxide ceramics produced by chemical vapor infiltration and reaction (CVI-R). *Journal of the European Ceramic Society*, 25 (6) 829–836.
6. Sieber, H., Cao, J., Rambo, C. R., (2008). Manufacturing of porous oxide ceramics from bioorganic preforms. *Advanced Ceramics, Materials, and Structures: B: Ceramic Engineering and Science Proceedings*, 23 (4) 175–181.
7. Cao, J., Rambo, C. R., Sieber, H., (2004). Preparation of porous Al₂O₃-ceramics by biotemplating of wood. *Journal of Porous Materials*, 11 163–172.
8. Faisal, M., Abu Tariq, M., Muneer, M., (2007). Photocatalysed degradation of two selected dyes in UV-irradiated aqueous suspensions of titania. *Dyes and Pigments*, 72 (2) 233–239.
9. Nogueira, R. F. P., Jardim, W. F., (1998). A fotocatalise heterogênea e sua aplicação ambiental. *Química Nova*, 21 (1) 69–72.
10. Tsoukleris, D. S., Kontos, A. I., Aloupogiannis, P., Falaras, P., (2007). Photocatalytic properties of screen-printed titania. *Catalysis Today*, 124 (3) 110–117.
11. Campoccia, D., Montanaro, L., Arciola, C. R., (2013). A review of the biomaterials technologies for infection-resistant surfaces. *Biomaterials*, 34 8533–8554.
12. Foster, H. A., Ditta, I. B., Varghese, S., Steele, A., (2011). Photocatalytic disinfection using titanium dioxide: spectrum and mechanism of antimicrobial activity. *Applied Microbiology and Biotechnology*, 90 (6) 1847–1868.
13. Faure, M., Gerardin, F., André, J.-C., Pons, M.-N., Zahraa, O., (2011). Study of photocatalytic damages induced on *E. coli* by different photocatalytic supports (various types and TiO₂ configurations). *Journal of Photochemistry and Photobiology A: Chemistry*, 222 (2) 323–329.
14. ISO 10678, (2010). Determination of photocatalytic activity of surfaces in an aqueous medium by degradation of methylene blue.
15. Alves, E. et al., (2008). Photodynamic inactivation of recombinant bioluminescent *Escherichia coli* by cationic porphyrins under artificial and solar irradiation. *The Journal of Industrial Microbiology and Biotechnology*, 35 (11) 1447–1454.
16. Brezová, V., Barbieriková, Z., Zukalová, M., Dvoranová, D., Kavan, L., (2014). EPR study of ¹⁷O-enriched titania nanopowders under UV irradiation. *Catalysis Today*, 230 112–118.
17. Li, M., Yin, J.-J., Wamer, W. G., Lo, Y. M., (2014). Mechanistic characterization of titanium dioxide nanoparticle-induced toxicity using electron spin resonance. *Journal of Food and Drug Analysis*, 22 (1) 76–85.
18. Billik, P. et al., (2007). Anatase TiO₂ nanocrystals prepared by mechanochemical synthesis and their photochemical activity studied by EPR spectroscopy. *Journal of Physics and Chemistry of Solids*, 68 (5) 1112–1116.
19. Kuk, S., Hwang, T., Yoon, Y., Kang, J., (2011). Evidence of singlet oxygen and hydroxyl radical formation in aqueous goethite suspension using spin-trapping electron paramagnetic resonance (EPR). *Chemosphere*, 84 (8) 1095–1101.
20. Chatterjee, D., Dasgupta, S., (2005). Visible light induced photocatalytic degradation of organic pollutants. *Journal of Photochemistry and Photobiology C: Photochemistry Reviews*, 6 (2) 186–205.
21. Krýsa, J., Musilová, E., Zita, J., (2011). Critical assessment of suitable methods used for determination of antibacterial properties at photocatalytic surfaces. *Journal of Hazardous Materials*, 195 100–106.